

Proton and Li-Ion Permeation through Graphene with Eight-Atom-Ring Defects

Eoin Griffin, Lucas Mogg, Guang-Ping Hao, Gopinadhan Kalon, Cihan Bacaksiz, Guillermo Lopez-Polin, T.Y. Zhou, Victor Guarochico, Junhao Cai, Christof Neumann, Andreas Winter, Michael Mohn, Jong Hak Lee, Junhao Lin, Ute Kaiser, Irina V. Grigorieva, Kazu Suenaga, Barbaros Özyilmaz, Hui-Min Cheng, Wencai Ren, Andrey Turchanin, Francois M. Peeters, Andre K. Geim,* and Marcelo Lozada-Hidalgo*



Cite This: *ACS Nano* 2020, 14, 7280–7286



Read Online

ACCESS |



Metrics & More



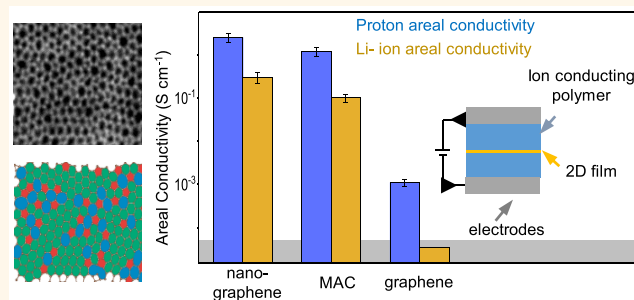
Article Recommendations



Supporting Information

ABSTRACT: Defect-free graphene is impermeable to gases and liquids but highly permeable to thermal protons. Atomic-scale defects such as vacancies, grain boundaries, and Stone–Wales defects are predicted to enhance graphene’s proton permeability and may even allow small ions through, whereas larger species such as gas molecules should remain blocked. These expectations have so far remained untested in experiment. Here, we show that atomically thin carbon films with a high density of atomic-scale defects continue blocking all molecular transport, but their proton permeability becomes ~ 1000 times higher than that of defect-free graphene. Lithium ions can also permeate through such disordered graphene. The enhanced proton and ion permeability is attributed to a high density of eight-carbon-atom rings. The latter pose approximately twice lower energy barriers for incoming protons compared to that of the six-atom rings of graphene and a relatively low barrier of ~ 0.6 eV for Li ions. Our findings suggest that disordered graphene could be of interest as membranes and protective barriers in various Li-ion and hydrogen technologies.

KEYWORDS: graphene, disorder, lithium ion, proton, fuel cell, battery



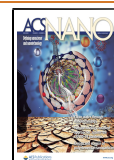
Despite being a one-atom-thick material, no more than a few gas atoms per hour can permeate through micrometer-sized defect-free graphene membranes, as proven experimentally.¹ Even the smallest ions are blocked by the crystal.² These phenomena arise because the dense electron clouds of graphene’s crystal lattice impose energy barriers of several electronvolts to incoming molecular and ionic species,^{3–5} which forbids their permeation under ambient conditions. In contrast, it has been shown experimentally that protons, nuclei of hydrogen atoms, can transport through defect-free graphene relatively easily, overcoming an energy barrier of only $\lesssim 1$ eV.^{1,2,6,7} In this context, theory predicts that modifying graphene’s lattice by introducing seven- or eight-atom rings should greatly reduce the energy barriers faced by protons³ and may even allow small ions (e.g., Li^+)⁴ to permeate. This is without losing graphene’s impermeability with respect to atoms and molecules.⁵ However, the permeability of such “extended” carbon rings remains untested experimentally, mostly because large enough graphene samples with high density of atomic-scale defects remained elusive. To

create defects, graphene crystals were previously perforated using ion irradiation or chemical and plasma etching.^{8–10} This approach results in a local loss of carbon atoms^{8–10} that typically form nanometer-sized pores⁸ rather than atomic-scale defects. These nanopores are permeable to gases,^{8,11} ions,⁸ and even macromolecules (e.g., DNA).^{8,12} An alternative approach is to grow materials with the required extended carbon-atom rings from the outset. Recently, high-quality one-atom-thick films with a high density of these eight-atom defects have been demonstrated using laser-assisted chemical vapor deposition¹³ and high-temperature quenching of metal foils in liquid hydrocarbon compounds.¹⁴ We refer to the latter two materials

Received: March 24, 2020

Accepted: May 19, 2020

Published: May 19, 2020



as disordered graphene (DG). Unlike irradiated graphene, DG presents a dense net of the “extended” carbon rings over the entire area, which allows for permeability studies of these ring structures. Below, we report proton and lithium-ion transport through disordered graphene grown using the methods reported previously.^{13,14}

RESULTS AND DISCUSSION

Material Characterization. To characterize the DG materials with atomic precision, we used transmission electron microscopy (TEM). The two-dimensional (2D) materials were suspended over circular apertures ($\sim 0.1\ \mu\text{m}$ in diameter) etched in free-standing silicon nitride (SiN) membranes (Supplementary Figure 1).⁶ Figure 1a,b shows that DG

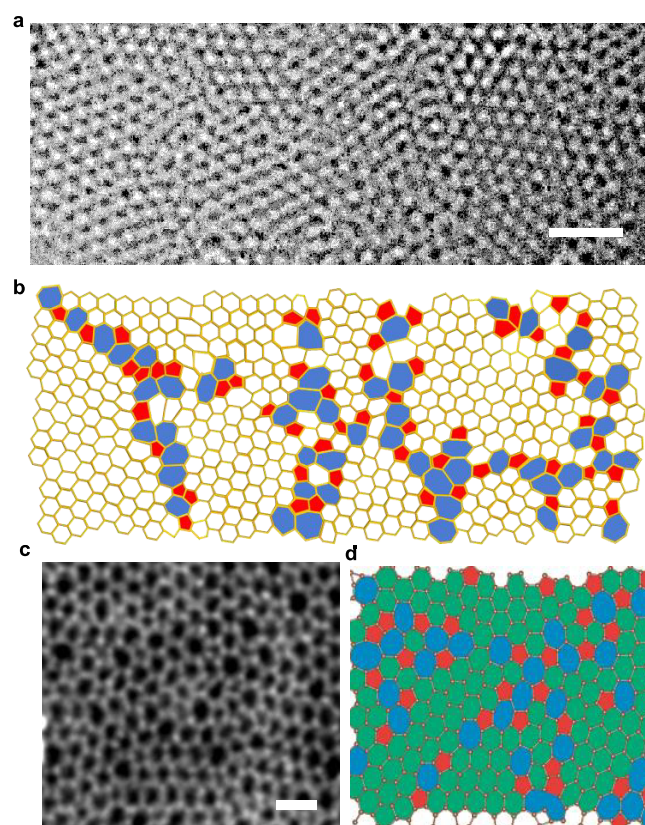


Figure 1. (a) High-resolution TEM micrograph of nanocrystalline graphene. Scale bar, 1 nm. (b) Schematic of the image in panel (a). Five-atom-ring structures are marked in red, six-atom rings in white with yellow boundaries, and both seven- and eight-atom rings in blue. (c) High-angle annular dark-field scanning TEM image of monolayer amorphous carbon. Scale bar, 0.5 nm. (d) Schematic of the image in (c). Red and green areas indicate five- and six-atom rings, respectively. The blue-colored areas denote seven- and eight-atom ring structures.

grown by quenching in liquid hydrocarbons¹⁴ can be described as a patchwork of nanometer-sized graphene crystallites. The grain boundaries of the material consist of five-, six-, seven-, and eight-atom rings. Because of the small domain size (3–4 nm), the material contains a large density of these non-hexagonal structures. We refer to this material as nanocrystalline graphene. On the other hand, DG synthesized *via* laser-assisted chemical vapor deposition¹³ consists of a one-atom-thick amorphous assembly of five-, six-, seven-, and eight-carbon-atom rings (Figure 1c,d), without any visible presence

of graphene crystallites. We refer to the material as monolayer amorphous carbon (MAC).¹³ The two DG films were compared with two other reference materials. The first one was an amorphous nanometer-thick carbon film referred to as a carbon nanomembrane (CNM). This material was synthesized by self-assembly of aromatic precursors that were cross-linked by electron irradiation, which resulted in short-range-order molecular nanosheets^{15,16} and a dense ($\sim 10^{14}\ \text{cm}^{-2}$) network of subnanometer ($\sim 0.7\ \text{nm}$ in diameter) pores piercing CNMs.¹⁶ In this work, we focused on ~ 0.9 and $1.2\ \text{nm}$ thick films from 1,1'-biphenyl-4-thiol and [1'',4',1',1]-terphenyl-4-thiol precursors, known as BPT-CNM and TPT-CNM, respectively (Supplementary Figure 2).¹⁵ The second reference material was defect-free graphene crystals obtained by mechanical exfoliation. Accordingly, our study compares the permeability of 2D carbon materials over the entire range of their possible disorder, from crystalline to disordered, to amorphous structures.

To further characterize the DG materials, we studied their mechanical properties. The suspended membranes were indented at their center with an atomic force microscope (AFM) tip, and the deflection, δ , of the membrane was recorded as a function of applied force, F . From the measured $F(\delta)$, it is possible to extract the 2D elastic (Young) modulus.¹⁷ The values were found to be ~ 190 and $100\ \text{N m}^{-1}$ for nanocrystalline graphene and amorphous carbon, respectively (Supplementary Figure 3). The reference graphene and CNM exhibited moduli of ~ 340 and $10\ \text{N m}^{-1}$, respectively, in agreement with the previous measurements.^{17,18} This shows that the rigidity of 2D carbon decreases with increasing disorder. Similarly, the mechanical strength also decreased by a factor of 6 for amorphous carbon compared to defect-free graphene (see “Mechanical properties of disordered graphene” in the Supporting Information). These changes are attributed to the presence of seven- and eight-atom rings, which weakens disordered graphene. Nevertheless, DG remains 10 times stronger than nanometer-thick carbon membranes. This can be attributed to the fact that DG is formed mainly by strong sp^2 carbon–carbon bonds,^{13,14} unlike CNM.¹⁵

Gas Transport Measurements. To find out whether the studied materials allow molecular transport, we measured their permeability with respect to helium, the most permeable gas. Before any measurements, our membranes were studied using atomic force and scanning electron microscopy. Membranes with cracks or other visible imperfections were discarded, and only the rest were tested for helium permeation (see “Device fabrication and characterization” in the Supporting Information). They separated two chambers. The feed chamber had a helium gas at a controllable pressure, and the permeate chamber was evacuated and connected to a mass spectrometer. Typically, the feed pressure was slowly increased up to a few tens of millibars to avoid damaging the membranes. No helium flow could be detected through either DG or CNM membranes within the accuracy of the mass spectrometer, which sets an upper bound for their helium permeance of $\sim 10^{-14}\ \text{mol s}^{-1}\ \text{cm}^{-2}\ \text{Pa}^{-1}$. This limit is comparable to, or even lower than, that of commercially available ion-conductive polymer membranes of $>100\ \mu\text{m}$ in thickness, which are optimized to block gas permeation (see “Gas transport measurements” in the Supporting Information).¹⁹

Ion Transport Measurements. These helium-tight carbon films should, in principle, be more permeable to

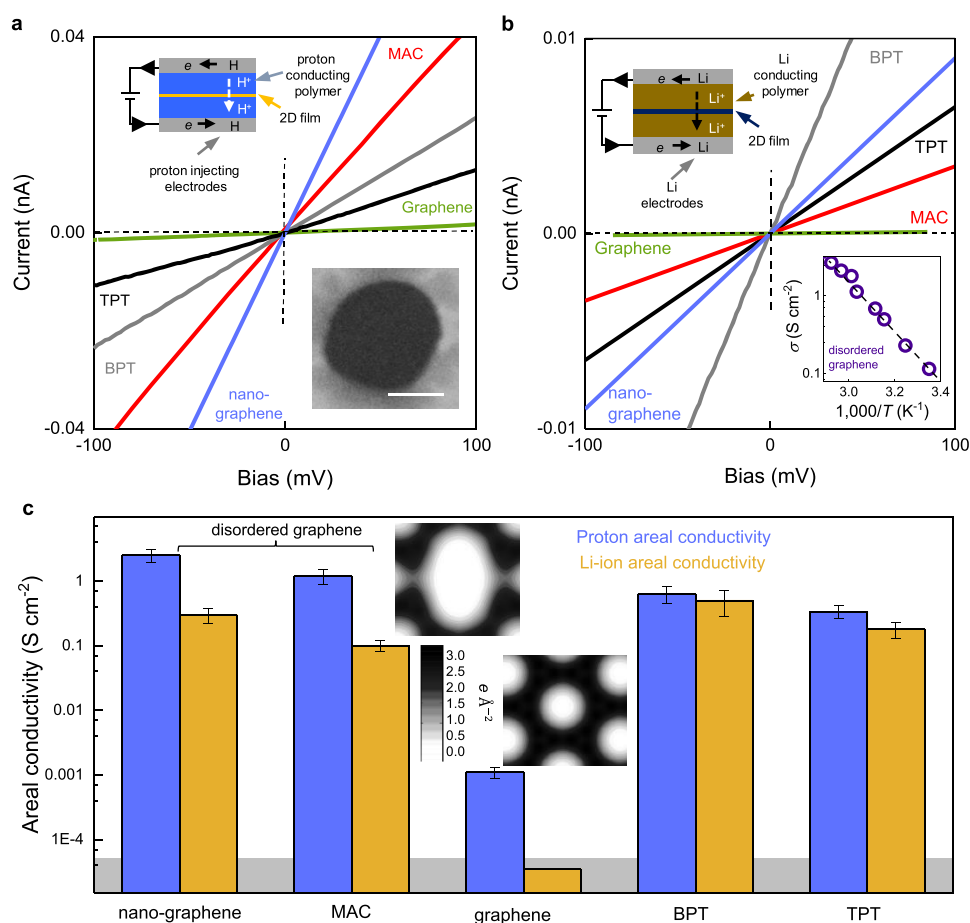


Figure 2. (a) Examples of I – V characteristics for proton transport through different carbon films (color coded). Nanographene stands for nanocrystalline graphene. Top inset: schematic of the experimental setup. Bottom inset: scanning electron micrograph of a suspended MAC membrane. The dark circular area in the image corresponds to the aperture in the SiN substrate over which the 2D film was suspended. Scale bar, 100 nm. (b) Examples of I – V characteristics found in Li-ion transport measurements. Top inset: device schematic. Bottom inset: Arrhenius plot for a typical DG membrane. Dotted line is used to guide the eye. (c) Statistics for proton (blue) and Li-ion (brown) areal conductivities measured for different 2D carbon films. Each bar shows the average for at least three different devices. Error bars are standard error of mean. The gray area indicates our detection limit given by parasitic leakage currents. Insets: charge density integrated along the direction perpendicular the graphene plane for a 5–8–5 defect (top) and defect-free graphene (bottom). The white areas represent minima in the electron density at the center of the ring structures.

protons than defect-free graphene because of their “looser” structures. To investigate proton permeation, the suspended membrane devices described above were coated on both sides with a proton-conducting polymer (Nafion²⁰) and electrically contacted with two proton injecting electrodes (inset of Figure 2a and Supplementary Figure 4), following the recipe reported previously.⁶ In this setup, the films effectively act as barriers between two semi-infinite proton reservoirs. To perform electrical measurements, the devices were placed in a humid H₂ atmosphere, which ensured the high proton conductivity of Nafion (see “Electrical measurements” in the Supporting Information).⁶ The current density I was found to vary linearly with small applied voltage V (Figure 2a), which allowed us to determine their areal conductivity, $\sigma = I/V$. We found that all disordered carbon films were ~ 1000 times more permeable than defect-free graphene.⁶ The most proton conductive was nanocrystalline graphene, closely followed (factor of ~ 2 lower) by MAC. Carbon nanomembranes (BPT-CNM and TPT-CNM) exhibited σ lower than MAC and $\sigma_{\text{BPT}}^{\text{H}} \sim 2\sigma_{\text{TPT}}^{\text{H}}$, which means their conductivities approximately scaled with their thicknesses. For reference, we measured devices with no carbon films placed over the apertures. Their resistance was

~ 100 times smaller than that of any device with the tested 2D carbon, which ensured that the resistance stemming from Nafion had a negligible contribution into the measured σ .

The high proton permeability of the disordered carbon films suggests that they could also be permeable to other ions. To investigate this possibility, we used Li ions, the penultimate smallest ion after the proton. In lithium transport experiments, suspended membranes were coated on both sides with a Li-conducting polymer²¹ and electrically connected to Li metal electrodes (see “Electrical measurements” in the Supporting Information). During assembly and electrical measurements, the devices were kept inside a glovebox containing an inert gas atmosphere (less than 1 ppm of either water or oxygen) to prevent Li from reacting. Figure 2b shows that I – V characteristics of all Li transport devices were linear. All of the 2D membranes were less permeable to Li ions than protons. BPT-CNM and TPT-CNM were the most Li-ion conductive of the tested materials displaying σ values rather close to the values found for proton transport, which means little selectivity between protons and Li ions. Again, their Li-ion conductance roughly scaled with their thickness. In contrast, the Li-ion conductivities for both DG materials

were ~ 10 times smaller than the corresponding values found for proton transport—that is, disordered graphene displayed large proton/Li-ion selectivity. For defect-free graphene, we could not discern any Li-ion transport through it, even if we increased the membrane areas by 2 orders of magnitude. Our sensitivity level of $\sim 10^{-13}$ A, given by leakage currents, translates the latter findings into an upper bound for Li-ion transport through defect-free graphene of $\sim 10^{-5}$ S cm $^{-2}$. As in the case of proton transport measurements, the lithium polymer was sufficiently conductive to contribute little into the reported σ (see “Electrical measurements” in the Supporting Information).

Our results suggest that the energy barriers for proton and Li-ion transport through disordered graphene should be lower than those of defect-free graphene. To quantify the barriers, we measured the temperature (T) dependence of σ between ~ 2 and 50 °C. This T range ensured adequate performance of the ion-conducting polymers^{20,21} and high reproducibility of $\sigma(T)$ between different devices and for consecutive heating and cooling cycles (Supplementary Figure 5). We found that Li-ion transport for both DG materials increased rapidly with T and could be described by the Arrhenius relation $\sigma \propto \exp(-E/kT)$ with the same activation energy, $E = 0.62 \pm 0.06$ eV, where k is the Boltzmann constant (Figure 2b, inset). For proton transport, $\sigma(T)$ was less reproducible between different devices at high T , and we had to limit our analysis to temperatures below room temperature. We attribute this to the fact that elevated temperatures are known to cause moisture loss in Nafion, which reduces its conductivity²⁰ and introduces a non-negligible series resistance. Even within the limited T range, we found that σ increased notably with T and could be fitted by $E \approx 0.4$ eV for both DG materials (Supplementary Figure 5). Note that, even at our highest T of 50 °C, Li-ion transport could not be detected through defect-free graphene. This is perhaps not surprising given the large activation energy of ~ 0.8 eV faced by small-size protons.⁶ A much higher barrier can be expected for larger Li ions,⁴ effectively forbidding Li-ion transport to be detectable.

The enhancement of proton and Li-ion permeability in DG with respect to defect-free graphene can be qualitatively understood from the perspective of electron clouds, which present transport barriers.⁶ The inset of Figure 2c shows that the electron clouds surrounding eight-atom-ring structures are notably sparser than those around six-atom rings. This should make the former rings more permeable to ions, as shown by similar analysis for graphene and hexagonal boron nitride.⁶ This interpretation is substantiated by density functional theory (DFT) calculations. We find that the energy barrier for both proton and Li-ion penetration through carbon-ring structures decreases with increasing number of atoms within the rings (Supplementary Figure 6), in agreement with previous theory results.^{3,4} Because of the exponential dependence of σ on E , proton and Li-ion transport through disordered graphene should probably be dominated by contributions from eight-atom rings, even if these were relatively rare.^{13,14} Our DFT calculations also explain why protons permeate ~ 10 times faster than Li ions through disordered graphene (Figure 2c). Eight-atom rings provide an energy barrier for incoming Li ions approximately two times higher than that for protons. This interpretation is also consistent with the absence of proton/Li-ion selectivity in carbon nanomembranes, which do not have eight-atom-ring structures but rather relatively large (~ 0.7 nm) pores. Indeed, σ measured for CNM scaled with

the thickness for both H and Li ions, indicating that the bulk transport is important, rather than the single entry–exit barrier presented by one-atom-thick graphene materials. The conclusion about bulk transport through CNMs is also consistent with their microscopic structures (effectively a dense network of subnanometer pores¹⁶) such that ions diffuse along tortuous trajectories as typical for porous media.²²

CONCLUSIONS

Besides providing fundamental insights into ion transport through 2D materials, disordered graphene is interesting in terms of applications. The DG materials reach technologically relevant proton conductivities at temperatures notably lower than those of defect-free graphene. Our experimental data show that the proton areal conductivity of disordered graphene at ~ 60 °C should exceed the industry benchmark set by Nafion 117 (~ 5 S cm $^{-2}$).²³ Defect-free graphene reaches this level only at ~ 200 °C. However, it is this latter temperature that is most desirable for fuel-cell operation.^{24–26} By extrapolation of the measured $\sigma(T)$, our DG membranes can reach ~ 100 S cm $^{-2}$ for this T range, well above the industry targets.²⁴ Importantly, disordered graphene can be mass produced,^{13,14} and fabricating large-area proton-conducting membranes should also be straightforward, as demonstrated for the case of defect-free graphene.²⁷ Furthermore, the lithium permeability of DG deserves special attention. Graphene is being explored as a material to host highly reactive Li–metal²⁸ and Li–Si particles²⁹ as anodes and Li–sulfur as cathodes³⁰ in batteries, in order to protect them from chemical reactions with electrolytes, prohibit Li dendritic growth, and provide mechanical stability. The key properties needed for the latter applications are high Li-ion conductivity combined with impermeability to reactive species. Because defect-free graphene is impermeable to Li ions, defects are essential, and those permeable only to Li ions (like eight-atom rings) offer considerable advantages. All of the above indicate that defect engineering in graphene and other 2D materials could be a productive venue for optimizing their use in energy conversion and storage technologies.

METHODS

Material Synthesis. Nanocrystalline graphene films were synthesized by quenching a Pt foil in liquid ethanol, as described in a recent report.¹⁴ Pt foil (99.95 wt %, 150 μ m thickness) was finely polished and annealed at 800 °C in air for 1 h as a cleaning step. After being heated at 900 °C in an argon atmosphere, the Pt foil was rapidly quenched in ethanol at room temperature to grow a large-area nanocrystalline graphene (NG) film.¹⁴ These films were then transferred on silicon oxide substrates using the electrochemical bubbling method.³¹ In brief, poly(methyl methacrylate) (PMMA) was spin-coated on a NG film with a Pt foil substrate. The PMMA-coated NG film/Pt foil was immersed into a NaOH (1 M) aqueous solution and used as a cathode. A Pt wire was used as an anode, and a constant electric current of 0.2 A was applied between the two electrodes. After the PMMA-coated NG film separated from the Pt substrate by hydrogen bubbles, it was cleaned in deionized water several times and collected onto a silicon oxide substrate. The PMMA was then dissolved in acetone and isopropyl alcohol.

Monolayer amorphous carbon films were synthesized by laser-assisted chemical vapor deposition (LCVD), as described in a recent report.¹³ Cu foils (35 μ m thick) were cleaned and annealed in a hydrogen atmosphere at 1010 °C. The foil was placed in the LCVD chamber, which was evacuated and then filled with methane gas. A plasma (350 kHz pulsed DC generator at 5 W) was turned on away from the sample, and the substrate was directly exposed to a pulsed

krypton fluoride laser ($40\text{--}75\text{ mJ cm}^{-2}$, 50 Hz). This process yields MAC films on both faces of the Cu foil. MAC films were then transferred onto silicon oxide substrates. To that end, one of the faces of the Cu foil was spin-coated with PMMA and the other face was exposed to oxygen plasma to remove the MAC film on that surface of the foil. The PMMA-coated MAC film/Cu foil was then placed in ammonium persulfate solution to dissolve the Cu foil. After being cleaned with deionized water several times, the MAC film was collected onto a silicon oxide substrate and the PMMA was dissolved.

Carbon nanomembranes were synthesized by low-energy electron irradiation of self-assembled aromatic molecular precursors.¹⁵ Au/mica substrates were placed in solutions of either 1'-biphenyl-4-thiol or [1'',4',1',1']-terphenyl-4-thiol precursors in dry degassed *N,N*-dimethylformamide. The precursor materials self-assembled on the Au surface, forming a continuous layer, due to the van der Waals interactions between the carbon atoms in the molecules. These self-assembled monolayers were then cross-linked by low-energy electron irradiation (50 eV , 50 mC/cm^2). The resulting films were spin-coated with PMMA. The mica substrate was then mechanically removed from the back of the Au foil, leaving the PMMA-coated carbon film/Au layer. The Au film was then dissolved in iodide solution. After several steps of cleaning in deionized water, the CNM was collected on a silicon oxide substrate and the PMMA was dissolved.

Electrical Measurements. Suspended membrane devices fabricated as described above were coated with ion-conducting polymers and ion-injecting electrodes. For proton transport devices, the membranes were coated with Nafion solution (5%, 1100 equiv weight) on both sides and then electrically connected with porous carbon electrodes containing a Pt catalyst (20% Pt on carbon). The devices were then baked at $130\text{ }^{\circ}\text{C}$ in a humid atmosphere to cross-link the polymer, as described in a previous report.⁶ For Li-ion transport, the suspended membrane devices were placed inside a glovebox containing less than 0.5 ppm of both water and oxygen. These were then coated on both sides with a standard lithium-conducting polymer, as described in previous reports of Li-ion studies in 2D material systems.^{32,33} The polymer used consisted of LiTFSI salt^{32,34} dissolved in poly(ethylene oxide) (PEO). To prepare the polymer, 0.05 g of LiTFSI and 0.3 g of powdered PEO (100,000 molecular weight) were dried overnight at 180 and $60\text{ }^{\circ}\text{C}$, respectively. These were then mixed in a 38:1 molar ratio with 2 mL of acetonitrile (99.8% anhydrous and further dried with 3 Å molecular sieves) and left to stir overnight at room temperature inside a glovebox, as described in a previous report. Devices were then electrically connected with Li metal electrodes. See [Supplementary Figure 4](#).

Electrical measurements of Li-ion transport devices were conducted inside the same glovebox used for their assembly. Proton transport devices, on the other hand, were placed inside a chamber containing a 10% H_2 in Ar gas atmosphere at 100% relative humidity. If our devices were left inside the measuring chambers (glovebox for Li ions and H_2 chamber for protons), these could be remeasured for weeks and even months after their assembly, just as with graphene devices. To measure the $I\text{--}V$ response of all devices, a Keithley 2636A sourcemeter was used to both apply voltage and measure current. Voltages were varied typically between $\pm 200\text{ mV}$ using sweep rates of $<0.1\text{ V min}^{-1}$.

Gas Transport Measurements. For gas transport measurements, suspended membrane devices ($\sim 1\text{ }\mu\text{m}$ diameter) without cracks or nanometer-sized imperfections were clamped with O-rings and used to separate two chambers built from standard vacuum components. One of these chambers (permeate) was connected to a mass spectrometer (Inficon UL200), and the other (feed) was equipped with an electrically controlled dosing valve, which allowed us to slowly introduce helium into the chamber. Both chambers were initially evacuated to a pressure of $\sim 10^{-2}\text{ mbar}$. Then, using the dosing valve, we controllably introduced helium gas into the feed chamber until the pressure reached a few tens of millibars. We normally did not apply higher pressures as this could cause some of the 2D suspended membranes to break and leak. Within this pressure range, we could not detect any gas transport at all within the sensitivity of our mass

spectrometer, $10^{-12}\text{ mbar l s}^{-1}$. The units from our mass spectrometer, mbar l s^{-1} , are straightforward to convert to mol s^{-1} using the ideal gas law. For the applied pressure and membrane area, the found gas transport upper bound translates into an upper bound to the maximum gas flow possible through these membranes as $\sim 10^{-14}\text{ mol s}^{-1}\text{ cm}^{-2}\text{ Pa}^{-1}$.

ASSOCIATED CONTENT

Supporting Information

The Supporting Information is available free of charge at <https://pubs.acs.org/doi/10.1021/acsnano.0c02496>.

Mechanical and transmission electron microscopy measurements of devices and density functional theory calculations ([PDF](#))

AUTHOR INFORMATION

Corresponding Authors

Andre K. Geim — Department of Physics and Astronomy & National Graphene Institute, The University of Manchester, Manchester M13 9PL, United Kingdom; Email: geim@manchester.ac.uk

Marcelo Lozada-Hidalgo — Department of Physics and Astronomy & National Graphene Institute, The University of Manchester, Manchester M13 9PL, United Kingdom; orcid.org/0000-0003-3216-7537; Email: marcelo.lozadahidalgo@manchester.ac.uk

Authors

Eoin Griffin — Department of Physics and Astronomy & National Graphene Institute, The University of Manchester, Manchester M13 9PL, United Kingdom

Lucas Mogg — Department of Physics and Astronomy & National Graphene Institute, The University of Manchester, Manchester M13 9PL, United Kingdom

Guang-Ping Hao — Department of Physics and Astronomy & National Graphene Institute, The University of Manchester, Manchester M13 9PL, United Kingdom; State Key Laboratory of Fine Chemicals, School of Chemical Engineering, Dalian University of Technology, Dalian 116024, China

Gopinadhan Kalon — Department of Physics and Astronomy & National Graphene Institute, The University of Manchester, Manchester M13 9PL, United Kingdom; Department of Physics, Indian Institute of Technology Gandhinagar, Gujarat 382355, India

Cihan Bacaksiz — Departement Fysica, Universiteit Antwerpen, B-2020 Antwerp, Belgium

Guillermo Lopez-Polin — Department of Physics and Astronomy & National Graphene Institute, The University of Manchester, Manchester M13 9PL, United Kingdom; Departamento de Física de la Materia Condensada, Universidad Autónoma de Madrid, 28049 Madrid, Spain

T.Y. Zhou — Shenyang National Laboratory for Materials Science, Institute of Metal Research, Chinese Academy of Sciences, Shenyang 110016, China

Victor Guarochico — Department of Physics and Astronomy & National Graphene Institute, The University of Manchester, Manchester M13 9PL, United Kingdom

Junhao Cai — Department of Physics and Astronomy & National Graphene Institute, The University of Manchester, Manchester M13 9PL, United Kingdom

Christof Neumann — Institute of Physical Chemistry and Center for Energy and Environmental Chemistry Jena (CEEC Jena), Friedrich Schiller University Jena, 07743 Jena, Germany

Andreas Winter – Institute of Physical Chemistry and Center for Energy and Environmental Chemistry Jena (CEEC Jena), Friedrich Schiller University Jena, 07743 Jena, Germany

Michael Mohn – Central Facility for Electron Microscopy, Electron Microscopy Group of Materials Science, Ulm University, Ulm 89081, Germany

Jong Hak Lee – Department of Physics, Department of Materials Science and Engineering & Centre for Advanced 2D Materials, National University of Singapore, Singapore 119260

Junhao Lin – National Institute of Advanced Industrial Science and Technology, Tsukuba, Japan & Department of Mechanical Engineering, The University of Tokyo, Bunkyo City, Tokyo 100-8921, Japan; Department of Physics, Southern University of Science and Technology, Shenzhen 518055, China;

orcid.org/0000-0002-2195-2823

Ute Kaiser – Central Facility for Electron Microscopy, Electron Microscopy Group of Materials Science, Ulm University, Ulm 89081, Germany

Irina V. Grigorieva – Department of Physics and Astronomy & National Graphene Institute, The University of Manchester, Manchester M13 9PL, United Kingdom

Kazu Suenaga – National Institute of Advanced Industrial Science and Technology, Tsukuba, Japan & Department of Mechanical Engineering, The University of Tokyo, Bunkyo City, Tokyo 100-8921, Japan

Barbaros Özyilmaz – Department of Physics, Department of Materials Science and Engineering & Centre for Advanced 2D Materials, National University of Singapore, Singapore 119260

Hui-Min Cheng – Shenyang National Laboratory for Materials Science, Institute of Metal Research, Chinese Academy of Sciences, Shenyang 110016, China; Shenzhen Graphene Center, Tsinghua-Berkeley Shenzhen Institute, Tsinghua University, Shenzhen 518055, China

Wencai Ren – Shenyang National Laboratory for Materials Science, Institute of Metal Research, Chinese Academy of Sciences, Shenyang 110016, China; orcid.org/0000-0003-4997-8870

Andrey Turchanin – Institute of Physical Chemistry and Center for Energy and Environmental Chemistry Jena (CEEC Jena), Friedrich Schiller University Jena, 07743 Jena, Germany;

orcid.org/0000-0003-2388-1042

Francois M. Peeters – Departement Fysica, Universiteit Antwerpen, B-2020 Antwerp, Belgium

Complete contact information is available at:

<https://pubs.acs.org/10.1021/acsnano.0c02496>

Notes

The authors declare no competing financial interest.

ACKNOWLEDGMENTS

The work was supported by the Lloyd's Register Foundation, EPSRC-EP/N010345/1, the European Research Council, the Graphene Flagship, the Deutsche Forschungsgemeinschaft project TRR 234 "CataLight" (Project B7, Grant No. 364549901), and the research infrastructure Grant No. INST 275/25 7-1 FUGG. E.G. and L.M. acknowledge the EPSRC NowNANO programme for funding.

REFERENCES

(1) Sun, P. Z.; Yang, Q.; Kuang, W. J.; Stebunov, Y. V.; Xiong, W. Q.; Yu, J.; Nair, R. R.; Katsnelson, M. I.; Yuan, S. J.; Grigorieva, I. V.; Lozada-Hidalgo, M.; Wang, F. C.; Geim, A. K. Limits on Gas Impermeability of Graphene. *Nature* **2020**, *579*, 229–232.

(2) Mogg, L.; Zhang, S.; Hao, G.-P.; Gopinadhan, K.; Barry, D.; Liu, B. L.; Cheng, H. M.; Geim, A. K.; Lozada-Hidalgo, M. Perfect Proton Selectivity in Ion Transport through Two-Dimensional Crystals. *Nat. Commun.* **2019**, *10*, 4243.

(3) Miao, M.; Nardelli, M. B.; Wang, Q.; Liu, Y. First Principles Study of the Permeability of Graphene to Hydrogen Atoms. *Phys. Chem. Chem. Phys.* **2013**, *15*, 16132–16137.

(4) Xin, Y.; Huang, A.; Hu, Q.; Shi, H.; Wang, M.; Xiao, Z.; Zheng, X.; Di, Z.; Chu, P. K. Barrier Reduction of Lithium Ion Tunneling through Graphene with Hybrid Defects: First-Principles Calculations. *Adv. Theory Simul.* **2018**, *1*, 1700009.

(5) Leenaerts, O.; Partoens, B.; Peeters, F. M. Graphene: A Perfect Nanoballoon. *Appl. Phys. Lett.* **2008**, *93*, 193107.

(6) Hu, S.; Lozada-Hidalgo, M.; Wang, F. C.; Mishchenko, A.; Schedin, F.; Nair, R. R.; Hill, E. W.; Boukhvalov, D. W.; Katsnelson, M. I.; Dryfe, R. A. W.; Grigorieva, I. V.; Wu, H. A.; Geim, A. K. Proton Transport through One-Atom-Thick Crystals. *Nature* **2014**, *516*, 227–230.

(7) Lozada-Hidalgo, M.; Hu, S.; Marshall, O.; Mishchenko, A.; Grigorenko, A. N.; Dryfe, R. A. W.; Radha, B.; Grigorieva, I. V.; Geim, A. K. Sieving Hydrogen Isotopes through Two-Dimensional Crystals. *Science* **2016**, *351*, 68–70.

(8) Wang, L.; Boutilier, M. S. H.; Kidambi, P. R.; Jang, D.; Hadjiconstantinou, N. G.; Karnik, R. Fundamental Transport Mechanisms, Fabrication and Potential Applications of Nanoporous Atomically Thin Membranes. *Nat. Nanotechnol.* **2017**, *12*, 509–522.

(9) Russo, C. J.; Golovchenko, J. A. Atom-By-Atom Nucleation and Growth of Graphene Nanopores. *Proc. Natl. Acad. Sci. U. S. A.* **2012**, *109*, 5953–5957.

(10) Kotakoski, J.; Krashennnikov, A. V.; Kaiser, U.; Meyer, J. C. From Point Defects in Graphene to Two Dimensional Amorphous Carbon. *Phys. Rev. Lett.* **2011**, *106*, 105505.

(11) Koenig, S. P.; Wang, L.; Pellegrino, J.; Bunch, J. S. Selective Molecular Sieving through Porous Graphene. *Nat. Nanotechnol.* **2012**, *7*, 728–732.

(12) Garaj, S.; Hubbard, W.; Reina, A.; Kong, J.; Branton, D.; Golovchenko, J. A. Graphene as a Subnanometre Trans-Electrode Membrane. *Nature* **2010**, *467*, 190–193.

(13) Toh, C.-T.; Zhang, H.; Lin, J.; Mayorov, A. S.; Wang, Y.-P.; Orofeo, C. M.; Ferry, D. B.; Andersen, H.; Kakenov, N.; Guo, Z.; Abidi, I. H.; Sims, H.; Suenaga, K.; Pantelides, S. T.; Özyilmaz, B. Synthesis and Properties of Free-Standing Monolayer Amorphous Carbon. *Nature* **2020**, *577*, 199–203.

(14) Zhao, T.; Xu, C.; Ma, W.; Liu, Z.; Zhou, T.; Liu, Z.; Feng, S.; Zhu, M.; Kang, N.; Sun, D.-M.; Cheng, H.-M.; Ren, W. Ultrafast Growth of Nanocrystalline Graphene Films by Quenching and Grain-Size-Dependent Strength and Bandgap Opening. *Nat. Commun.* **2019**, *10*, 4854.

(15) Turchanin, A.; Götzhäuser, A. Carbon Nanomembranes. *Adv. Mater.* **2016**, *28*, 6075–6103.

(16) Yang, Y.; Dementyev, P.; Biere, N.; Emmrich, D.; Stohmann, P.; Korzetz, R.; Zhang, X.; Beyer, A.; Koch, S.; Anselmetti, D.; Götzhäuser, A. Rapid Water Permeation through Carbon Nanomembranes with Sub-Nanometer Channels. *ACS Nano* **2018**, *12*, 4695–4701.

(17) López-Polín, G.; Gómez-Navarro, C.; Parente, V.; Guinea, F.; Katsnelson, M. I.; Pérez-Murano, F.; Gómez-Herrero, J. Increasing the Elastic Modulus of Graphene by Controlled Defect Creation. *Nat. Phys.* **2015**, *11*, 26–31.

(18) Zhang, X.; Beyer, A.; Götzhäuser, A. Mechanical Characterization of Carbon Nanomembranes from Self-Assembled Monolayers. *Beilstein J. Nanotechnol.* **2011**, *2*, 826–833.

(19) Schalenbach, M.; Hoefner, T.; Paciok, P.; Carmo, M.; Lueke, W.; Stolten, D. Gas Permeation through Nafion. Part 1: Measurements. *J. Phys. Chem. C* **2015**, *119*, 25145–25155.

(20) Mauritz, K. A.; Moore, R. B. State of Understanding of Nafion. *Chem. Rev.* **2004**, *104*, 4535–4586.

(21) Fergus, J. W. Ceramic and Polymeric Solid Electrolytes for Lithium-Ion Batteries. *J. Power Sources* **2010**, *195*, 4554–4569.

- (22) Wiedenmann, D.; Keller, L.; Holzer, L.; Stojadinovic, J.; Munch, B.; Suarez, L.; Fumey, B.; Hagendorfer, H.; Bronnimann, R.; Modregger, P.; Gorbar, M.; Vogt, U. F.; Zuttel, A.; Mantia, F. L.; Wepf, R.; Grobety, B. Three-Dimensional Porous Structure and Ion Conductivity of Porous Ceramic Diaphragms. *AIChE J.* **2013**, *59*, 1446–1457.
- (23) Casciola, M.; Alberti, G.; Sganappa, M.; Narducci, R. On the Decay of Nafion Proton Conductivity at High Temperature and Relative Humidity. *J. Power Sources* **2006**, *162*, 141–145.
- (24) U.S Department of Energy. Multi-Year Research, Development and Demonstration Plan; https://www.energy.gov/sites/prod/files/2014/12/f19/fcto_myrrdd_full_document.pdf (accessed 2018-06-01).
- (25) Bose, S.; Kuila, T.; Nguyen, T. X. H.; Kim, N. H.; Lau, K.-T.; Lee, J. H. Polymer Membranes for High Temperature Proton Exchange Membrane Fuel Cell: Recent Advances and Challenges. *Prog. Polym. Sci.* **2011**, *36*, 813–843.
- (26) Zhang, Y.; Knibbe, R.; Sunarso, J.; Zhong, Y.; Zhou, W.; Shao, Z.; Zhu, Z. Recent Progress on Advanced Materials for Solid-Oxide Fuel Cells Operating Below 500 °C. *Adv. Mater.* **2017**, *29*, 1700132.
- (27) Lozada-Hidalgo, M.; Zhang, S.; Hu, S.; Esfandiari, A.; Grigorieva, I. V.; Geim, A. K. Scalable and Efficient Separation of Hydrogen Isotopes Using Graphene-Based Electrochemical Pumping. *Nat. Commun.* **2017**, *8*, 15215.
- (28) Zhao, J.; Zhou, G.; Yan, K.; Xie, J.; Li, Y.; Liao, L.; Jin, Y.; Liu, K.; Hsu, P.-C.; Wang, J.; Cheng, H.-M.; Cui, Y. Air-Stable and Freestanding Lithium Alloy/Graphene Foil as an Alternative to Lithium Metal Anodes. *Nat. Nanotechnol.* **2017**, *12*, 993–999.
- (29) Li, Y.; Yan, K.; Lee, H.-W.; Lu, Z.; Liu, N.; Cui, Y. Growth of Conformal Graphene Cages on Micrometre-Sized Silicon Particles as Stable Battery Anodes. *Nat. Energy* **2016**, *1*, 15029.
- (30) Tan, G.; Xu, R.; Xing, Z.; Yuan, Y.; Lu, J.; Wen, J.; Liu, C.; Ma, L.; Zhan, C.; Liu, Q.; Wu, T.; Jian, Z.; Shahbazian-Yassar, R.; Ren, Y.; Miller, D. J.; Curtiss, L. A.; Ji, X.; Amine, K. Burning Lithium in CS₂ for High-Performing Compact Li₂S-Graphene Nanocapsules for Li-S Batteries. *Nat. Energy* **2017**, *2*, 17090.
- (31) Gao, L.; Ren, W.; Xu, H.; Jin, L.; Wang, Z.; Ma, T.; Ma, L.-P.; Zhang, Z.; Fu, Q.; Peng, L.-M.; Bao, X.; Cheng, H.-M. Repeated Growth and Bubbling Transfer of Graphene with Millimetre-Size Single-Crystal Grains Using Platinum. *Nat. Commun.* **2012**, *3*, 699.
- (32) Zhao, S. Y. F.; Elbaz, G. A.; Bediako, D. K.; Yu, C.; Efetov, D. K.; Guo, Y.; Ravichandran, J.; Min, K.-A.; Hong, S.; Taniguchi, T.; Watanabe, K.; Brus, L. E.; Roy, X.; Kim, P. Controlled Electrochemical Intercalation of Graphene/h-BN van der Waals Heterostructures. *Nano Lett.* **2018**, *18*, 460–466.
- (33) Kühne, M.; Börrnert, F.; Fecher, S.; Ghorbani-Asl, M.; Biskupek, J.; Samuelis, D.; Krashennnikov, A. V.; Kaiser, U.; Smet, J. H. Reversible Superdense Ordering of Lithium between Two Graphene Sheets. *Nature* **2018**, *564*, 234–239.
- (34) Kalhoff, J.; Bresser, D.; Bolloli, M.; Alloin, F.; Sanchez, J.-Y.; Passerini, S. Enabling LiTFSI-Based Electrolytes for Safer Lithium-Ion Batteries by Using Linear Fluorinated Carbonates as (Co)Solvents. *ChemSusChem* **2014**, *7*, 2939–2946.